Elsevier Editorial System(tm) for Catalysis Today

Manuscript Draft

Manuscript Number: CATTOD-D-16-00631R2

Title: Understanding the differences in catalytic performance for hydrogen production of Ni and Co supported on mesoporous SBA-15

Article Type: SI: Environmental Catalysis-2016

Keywords: Nickel cobalt catalysts; in situ XPS; Hydrogen production; DRM Methane reforming.

Corresponding Author: Professor Alfonso Caballero,

Corresponding Author's Institution: University of Seville

First Author: Alfonso Caballero

Order of Authors: Alfonso Caballero; Alberto Rodriguez-Gomez; Rosa Pereñiguez

Abstract: Three mono and bimetallic NixCo1-x/SBA-15 catalysts (x=1, 0.5 and 0) with a total metallic content of 10 wt% have been prepared by a deposition-precipitation (DP) method. The catalytic performances on the dry reforming of methane reaction (DRM) have been determined and correlated with their physical and chemical state before and after the catalytic reaction. So, while the nickel monometallic system presents a high activity and stability in the DRM reaction, the Co/SBA-15 catalytic system turns out completely inactive. For its part, the Ni0.5Co0.5/SBA-15 has initially a catalytic performance similar to the Ni/SBA-15 monometallic system, but rapidly evolving to an inactive system, therefore resembling the behavior of the cobalt-based catalyst. The characterization by TEM and in situ XPS techniques has allowed us to ascribe these differences to the initial state of metallic particles after reduction and their different evolution under reaction conditions. So, while after reduction both nickel containing NixCo1-x/SBA-15 catalysts (x=1 and 0.5) present a well dispersed metallic phase, the cobalt monometallic catalyst yields big metallic particles with a heterogeneous distribution of sizes. Additionally, unlike the Ni/SBA-15, the NiCo/SBA 15 system increases during reaction the metallic particle sizes.
Besides indicating that the particle size is a major reason determining the catalytic performances, these results suggest that in the Ni-Co system both metals form after reduction a bimetallic phase mainly located inside the mesoporous channels of SBA-15 support. Under DRM reaction conditions, the cobalt is segregated to the surface of the bimetallic particles, which seems to determine the interaction with the support surface SBA-15. This feature gives rise to a much less stable metallic phase which suffers an important sintering process under DRM catalytic conditions.

Highlights

- **Ni-Co/SBA-15 catalysts has been prepared from highly dispersed Ni/Co silicate**
- **Nickel yields a high dispersed metallic phase and a stable catalytic performance**
- **A bimetallic phase is formed mainly located in the channels of SBA-15 support**
- **Co segregation to the surface destabilizes and increases the particle size**

*Graphical Abstract (for review)

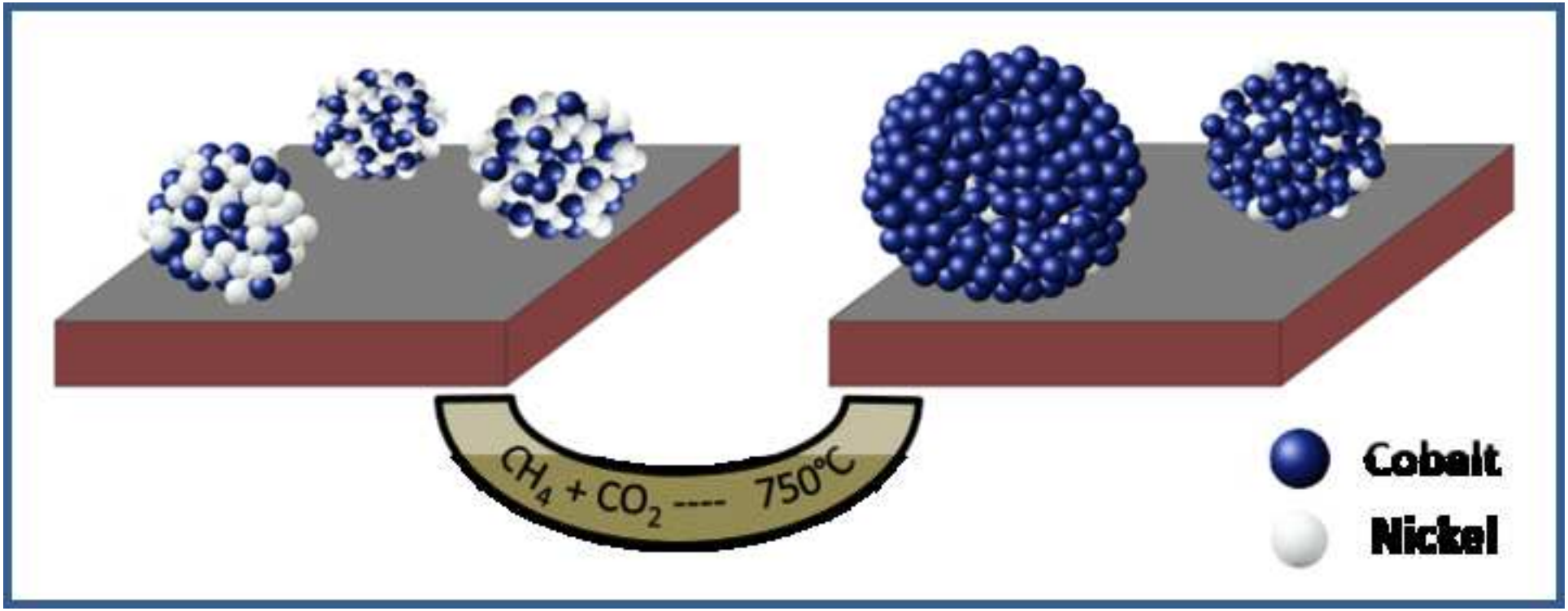

Understanding the differences in catalytic performance for hydrogen production of Ni and Co supported on mesoporous SBA-15

Alberto Rodriguez-Gomez, Rosa Pereñiguez and Alfonso Caballero*
Instituto de Ciencia de Materiales de Sevilla (CSIC-University of Seville) and Departamento de Quimica Inorganica, University of Seville. Avda. Américo Vespucio, 49. 41092. Seville, Spain. caballero@us.es

Abstract

Three mono and bimetallic Ni_xCo_{1-x}/SBA-15 catalysts (x=1, 0.5 and 0) with a total metallic content of 10 wt% have been prepared by a deposition-precipitation (DP) method. The catalytic performances on the dry reforming of methane reaction (DRM) have been determined and correlated with their physical and chemical state before and after the catalytic reaction. So, while the nickel monometallic system presents a high activity and stability in the DRM reaction, the Co/SBA-15 catalytic system turns out completely inactive. For its part, the $Ni_{0.5}Co_{0.5}$/SBA-15 has initially a catalytic performance similar to the Ni/SBA-15 monometallic system, but rapidly evolving to an inactive system, therefore resembling the behavior of the cobalt-based catalyst. The characterization by TEM and *in situ* XPS techniques has allowed us to ascribe these differences to the initial state of metallic particles after reduction and their different evolution under reaction conditions. So, while after reduction both nickel containing Ni_xCo_{1-x}/SBA-15 catalysts (x=1 and 0.5) present a well dispersed metallic phase, the cobalt monometallic catalyst yields big metallic particles with a heterogeneous distribution of sizes. Additionally, unlike the Ni/SBA-15, the NiCo/SBA-15 system increases during reaction the metallic particle sizes.

Besides indicating that the particle size is a major reason determining the catalytic performances, these results suggest that in the Ni-Co system both metals form after reduction a bimetallic phase mainly located inside the mesoporous channels of SBA-15 support. Under DRM reaction conditions, the cobalt is segregated to the surface of the bimetallic particles, which seems to determine the interaction with the support surface SBA-15. This feature gives rise to a much less stable metallic phase which suffers an important sintering process under DRM catalytic conditions.

Keywords: Nickel cobalt catalysts, *in situ* XPS, Hydrogen production, DRM Methane reforming.

1. Introduction

Supported nickel catalytic systems are currently one of the most important industrial heterogeneous catalysts because its remarkable performance in a number of economically strategic processes [1-5]. Among them, the steam reforming of methane (SRM, $CH_4 + H_2O \leftrightarrow 3H_2 + CO$) can be outlined as the main industrial process for obtaining hydrogen and synthesis gas, used to synthesize various important chemicals and fuels [6-9]. Although it is not yet commercially exploited, the dry reforming of methane (DRM, $CH_4 + CO_2 \leftrightarrow 2H_2 + 2CO$) is an especially interesting reaction that transforms two of the most harmful greenhouse gases, methane and carbon dioxide, into a mixture of hydrogen and carbon monoxide [10-12]. Once again, Ni-based catalysts are the most widely tested in the literature for this reforming reaction, even though noble metal based catalysts such as Pt, Ru and Rh are much more performance toward methane conversion. The principal issue comes from the fact that Ni typically undergoes severe deactivation processes, mainly due to coke formation, but also due to sintering of the metallic phase, generating big metallic particles which at the same time, favors the coke formation processes [13-17]. As an alternative to overcome these issues, a number of publications have shown as the use of bimetallic systems, as the combination of nickel and cobalt modified the catalytic performance in steam and dry reforming of methane [18-23]. But, depending on the support or the preparation methods both effects, improvements and worsening of the efficiency, have been reported. Main reasons explaining these contradictory findings are probably related with differences in the interaction of metals with support surface, which has been recognized as an essential factor affecting the stability of metal [24-26]. So, a strategy to avoid the growth of metallic particles is the use of special supports, and in particular mesoporous supports. These supports typically have high surface area and a tailored size of the porosity, which can be used to control the size of the metallic particles [27-29].

In this work we have prepared three catalysts containing nickel and/or cobalt supported on the mesoporous silica SBA-15. The catalytic systems, with a total metal loading of 10 wt%, has been prepared by means of a deposition-precipitation method (Ni_xCo_{1-x}/SBA-15 catalysts, x=1, 0.5 and 0). As the catalytic behavior of these systems are pretty different, we have characterized the catalytic systems after hydrogen reduction and after dry reforming reaction conditions using among others, *in situ* XPS and TEM. The obtained results have allowed us to correlate the catalytic performances with both, the initial state of metallic phases after reduction, and the final state of these metallic particles after DRM reaction. The interaction of the metallic phase with the SBA-15 inner surface appears as a major factor determining the catalytic stability of these Ni_xCo_{1-x}/SBA-15 catalysts.

2. Experimental

Catalysts preparation

The mesoporous silica SBA-15 used as support was prepared according to a method previously described in the literature [30-31]. Summarizing, 18 g of P123 was dissolved in 270 mL of distilled water and afterwards a solution of 675 mL of HCl 2.5 M was added and heated up to 50 °C. Next, an amount of TEOS was added and kept at 50 °C for 18 h. The product obtained was filtered, washed with boiling distilled water, dried under vacuum at 70 °C and calcined on for 3 hours at 550 °C.

The cobalt and nickel metal phases were supported on SBA-15 by a deposition-precipitation method (DP) using urea as a precipitant agent according to the method described by Liu et al. [32]. 1 gram of calcined SBA-15 was dispersed in HNO_3 0.01 M with the required amount of metal precursors $Ni(NO_3)_2{\cdot}6H_2O$ and/or $Co(NO_3)_3{\cdot}6H_2O$. On stirring, an amount of urea was added and the temperature increased up to 105 °C. After 2 hours, the mix was cooled down to room temperature and the powder filtered and dried at 110 °C for 24 h. Finally, it was submitted to a calcination treatment on air at 550 °C. The resulting products were labeled as 10%Ni/SBA-15, 10%Co/SBA-15 and 5%Ni-5%Co/SBA-15. In order to clarify the effect of the preparation treatment, a similar procedure was accomplished without metals addition, and the sample was labeled as SBA-15-DP.

X-ray diffraction (XRD)

The XRD analysis of calcined and reduced samples were recorded in a PANalytical X-Pert PRO diffractometer with a Cu source (λ=1.5418 Å, Cu Kα), working in a Bragg-Brentano configuration and equipped with an X'Celerator Detector (active range of 2 = 2.18°). The data acquisition was carry out in a 2θ range of 10-80°, a step of 0.05° and an acquisition time of 240 s.

Temperature Programmed Reduction (TPR)

The temperature-programmed reduction profiles were obtained using a thermal conductivity detector based in a Wheatstone bridge. The hydrogen consumption was previously calibrated using commercial CuO. A 5% H_2/Ar calibrated mix was used as both carrier and reference gas, with a typical flow rate of 50 $mL \cdot min^{-1}$. Following the recommendation to avoid peak coalescence [33], the experimental conditions were chosen to assure a total hydrogen consumption of approximately 100 µmol of H_2. Typically, the experiment was carried out from room temperature up to 1000 °C using a heating ramp of 10 °C·min-1.

Transmission Electronic Microscopy (TEM)

TEM images were obtained in a Philips CM200 microscope operating at 200 kV. Samples were dispersed on ethanol and deposited onto a copper grid coated with a lacey carbon film. Histograms for particle size distribution were obtained by sampling around 150 particles.

X-ray absorption spectroscopy (XAS)

XAS (EXAFS and XANES regions) were recorded at the BL22 beamline (CLAESS) of ALBA synchrotron and the BM25A beamline (SPLINE) of ESRF synchrotron facilities. The required amount of sample to maximize the signal/noise ratio was pelletized and XAS spectra collected at RT after calcination. Standards Ni and Co foils were measured and used for energy calibration. The XAS spectra of Ni K-edge and Co K-edge were recorded for a 1000 eV interval, with a step of 0.5 eV step across the XANES region. Once extracted from the XAS spectra, the EXAFS oscillations were Fourier transformed

(F.T.) in the range 2.4–11.0 $Å^{-1}$. Spectra were analyzed using the software package IFEFFIT [34].

X-ray photoelectron spectroscopy (XPS)

XPS experiments were carried out in a VG-ESCALAB 210 equipment over pelletized samples. Samples were introduced in a pre-chamber at 10^{-7} Torr. Acquisition was performed in an appendant analysis chamber equipped with a SPECS Phoibos 100 hemispheric analyzer at 10^{-9} Torr using Mg Kα radiation (E=1.5418 keV) with 20 mA of anode current and 12 kV of potential acceleration. Before acquisition, each sample was treated *in situ* at different temperatures (RT, 350, 500 and 750 °C) in a flow of 5% H_2/Ar at atmospheric pressure using a cell chamber attached to the abovementioned pre-chamber.

Catalytic activity tests

Dry reforming of methane (DRM) tests were performed using 20 mg of catalyst held in a tubular quartz reactor through wool quartz. The catalytic systems were pre-treated in 5% H_2/Ar at 750 °C for 1 h with a heating ramp of 10 °C·min^{-1}. Reaction was carried out with a not diluted mix (1:1) of 40 mL·min^{-1} of CH_4 and 40 mL·min^{-1} of CO_2 at 750 °C during 42 h. Reaction products were analyzed by GC using an Agilent´s 490 microGC equipped with three micro-columns and TCD detectors.

3. Results and discussion

3.1. Characterization of fresh calcined systems

The three catalytic systems were characterized by N_2 adsorption analysis (BET, BJH), XRD, TEM, TPR, XAS and XPS. As expected for mesoporous materials, all samples exhibited type-IV adsorption isotherms. However, as reflected in Table 1, they undergo a significant change in BET surface area and mean porous size as a consequence of the alkaline treatment during the DP preparation methodology. Every sample, including a blank SBA-15 support submitted to the DP treatment without metal salts in solution (SBA-15-DP), suffers a decrease in surface area of around 65%, from 738 $m^2.g^{-1}$ of the pristine SBA-15 to 250-280 $m^2.g^{-1}$. Simultaneously, the smaller porosity collapses

(mean size increasing from 6.7 to 10-12 nm). Despite this loss of surface area, the analysis by TEM (Figure 1) shows that the channeled structure of the SBA-15 support is preserved [35]. The calcined Ni_xCo_{1-x}/SBA-15 catalysts present the characteristic "fibrous" structures of phyllosilicate phases, previously found in similar systems [36-40]. The ascription of these fibrous shapes to phyllosilicate is confirmed by the XRD diagrams included in Figure 2a. According to the database and previous works [38], the wide peaks appearing around 35 and 61^o correspond to nickel and/or cobalt silicate hydroxide. In no case, peaks from Ni or Co oxides phases could be detected. It is worthy to note the intermediate position at about 60.5^o observed for the bimetallic $Ni_{0.5}Co_{0.5}$/SBA-15 catalysts, which can be an indication of the formation of a bimetallic nickel cobalt phyllosilicate phase. The formation of these silicates in the calcined samples is also confirmed by XAS spectroscopy. The XANES spectrum and Fourier Transforms of EXAFS regions included in Figure 3 clearly differ from those of typical nickel and cobalt oxides, and resemble those previously identified as silicates [3, 41,42].

3.2. Characterization of reduced catalytic systems

Figure 2 also includes the diffraction patterns of the three Ni_xCo_{1-x}/SBA-15 catalysts after a reduction treatment in hydrogen at 750 ^{o}C. In all cases, the diagrams show new diffraction peaks around 44.5 and 52^o that can be ascribed to reduced nickel and/or cobalt phases. As detailed in Figure 2b, the position and intensity of peak around 44-45^o corresponding to (111) reflection of the cubic Ni and/or Co phases, slightly differs between samples: 44.3^o for reduced Co/SBA-15, 44.6^o for Ni/SBA-15, and an intermediate value for the NiCo/SBA-15 catalyst, which once again suggests the formation of a Ni-Co bimetallic phase. The TPR profiles included in Figure 4 show also interesting differences between the reduction processes of the three catalytic systems. The Ni/SBA-15 sample presents a main peak centered at 660 ^{o}C, previously assigned to a nickel phyllosilicate phase [40,41], with a small shoulder at lower temperature, around 400 ^{o}C. According to previous results obtained by our group, these two reduction features can be respectively ascribed to the reduction of oxidized nickel located inside and outside the mesoporous channels of SBA-15 support [40]. For its part, the bimetallic NiCo/SBA-15 catalyst presents a similar profile, but shifted to

higher temperature (peaks maximum at 700 ^{o}C and 500 ^{o}C, respectively). These similitudes suggest that also in this system the metals could be located both in the inner and outer surface of support. The formation of a bimetallic silicate with a stronger interaction with the support can explain the higher reduction temperature observed by TPR. Finally, as expected [43], the Co/SBA-15 catalyst reduces at higher temperature, presenting at least two peaks centered at 750 and 850 ^{o}C.

The metallic particles obtained after the reduction treatment can be visualized in Figure 5. Both nickel containing samples, Ni/SBA-15 (Figure 5a) and NiCo/SBA-15 (Figure 5b) generate small and homogeneous nickel particles of about 4-6 nm (Table 1), slightly bigger for the bimetallic catalyst. From the visual inspection of these two TEM images, it is evident that many metal particles appear aligned with the mesoporous channels of support, once again suggesting that they could be located inside the mesoporous [40]. On the contrary, the TEM image of Co/SBA-15 (Figure 5c) shows bigger heterogeneous particles with a mean diameter around 13-15 nm (Table 1), necessarily located outside the mesopores of support. Additionally, the image shows the presence of much smaller particles.

The reduction processes of these three SBA-15 supported catalysts have been studied by means of *in situ* XPS spectroscopy under a hydrogen atmosphere at 350, 500 and 750 ^{o}C. Figure 6 includes the XPS obtained for the monometallic Ni/SBA-15 (Ni 2p region) and Co/SBA-15 (Co 2p region), while the Figure 7 gathers the respective regions of the bimetallic NiCo/SBA-15 catalysts (Ni 2p and Co 2p regions). In all cases, the reduction treatment at 350 ^{o}C does not provoke noticeable changes while the use of the higher reduction temperature (750 ^{o}C) gives rise in all catalysts to well reduced metallic nickel and cobalt phases. However, interesting differences of behavior can be observed after reduction in hydrogen at 500 ^{o}C. At this temperature nickel appears completely reduced in Ni/SBA-15 and NiCo/SBA-15 catalysts. As the TPR profiles in Figure 4 indicated that after this treatment most of metal should remain oxidized, the undetected oxidized nickel must be located inside the mesoporous channels in both catalysts, which are invisible for XPS, a surface sensitive technique. So, as found previously for different preparation methods [40], the deposition-precipitation methodology seems to favor the confinement of nickel inside the porous of SBA-15. Regarding the state of cobalt, in the monometallic Co/SBA-15 catalysts it remains

basically unreduced after hydrogen treatment at 500 ^{o}C, as can be expected from the TPR of Figure 4. However, from the Co 2p XPS signal, it can be estimated that a small fraction of about 10% is reduced to the metallic state. Taking into account that XPS only detects the metal located in the external surface of SBA-15, the reduced fraction at 500 ^{o}C must be located in the outer surface of SBA-15. More interesting is the fact that cobalt is much more reducible in the bimetallic NiCo/SBA-15 catalyst. A similar estimation of Co 2p XPS signal of Figure 7, allows estimating that around 65% of cobalt is reduced to the metallic state at 500 ^{o}C. According to TPR in Figure 4, only the shoulder at low temperature is affected by this treatment at 500 ^{o}C, which represents less than 5% of total cobalt content. Once again, considering the surface sensitivity of XPS, it can be concluded that in the bimetallic NiCo/SBA-15 catalyst most of the cobalt particles must be located into the channels of the SBA-15 support, which remain oxidized but are invisible for XPS.

3.3. Catalytic studies

The catalytic activity of the three catalytic systems was studied under dry reforming reaction of methane (DRM) conditions. As depicted in Figure 8, the catalytic performances are completely different depending on the metals presented in the catalysts. Face to the outstanding activity and stability of Ni/SBA-15, which maintains its catalytic properties during the 48 h period of DRM reaction, Co/SBA-15 is completely inactive with absolutely no conversion of methane from the very beginning of reaction.

In a certain way, the bimetallic NiCo/SBA-15 presents a dual catalytic behavior. The initial activity is not much less than half of the initial Ni/SBA-15 activity (30% vs. 73% conversion of methane), as could be expected considering the relative nickel content of these two catalysts (10 and 5%, respectively) and the slightly higher particle size in the bimetallic NiCo/SBA-15 catalyst after reduction (Figure 5). But the bimetallic system loses completely the activity after 5 h on stream, resembling now the catalytic behavior of Co/SBA-15 monometallic catalyst.

After the DRM reaction, the catalysts present the appearance showed in the TEM images of Figure 9. The metallic particles essentially maintain their size and

distribution of the freshly reduced Ni/SBA-15 (4-6 nm) and Co/SBA-15 (13-15 nm) catalysts (see Table 1, Figures 5a, 5c and 9a, 9c, respectively), which can be related with the stable catalytic performance of both catalysts over time (Figure 8). In particular, the high stability of nickel agrees with that previously observed by other authors in similar systems [37]. On the contrary the image in Figure 9b clearly shows that metallic particles of bimetallic NiCo/SBA-15 have increased their mean size, from 6 nm of the freshly reduced catalyst to about 8 nm after DRM reaction. Once again this behavior seems to be correlated with the observed evolution in the catalytic performance, initially similar to that of monometallic nickel one, and finally reaching that of the cobalt monometallic system. This increase in size indicates that the interaction with support of bimetallic NiCo/SBA-15 and monometallic Ni/SBA-15 differs, strong in the monometallic, which maintains the nickel particle size, and much less intense in the bimetallic system. This different behavior suggests that after reduction of the bimetallic catalyst the nickel is responsible for the interaction with support (which assures tiny metallic particles in both catalyst), but under reaction conditions cobalt is preferentially segregated to the surface of bimetallic particles, which weakens the interaction with support, favoring the sintering processes.

4. Conclusions

In this work we have studied the state and catalytic performance of three Ni_xCo_{1-x}/SBA-15 catalysts prepared by a deposition-precipitation method. Combining the physical and chemical state of these systems with the catalytic behavior, it has been stablished a clear correlation between the outstanding catalytic performance of nickel with the strong interaction of 5 nm metallic particles mainly located into the mesoporous channels of SBA-15, which remain unchanged during the 48 h period under DRM reaction conditions. On the contrary, upon hydrogen reduction the monometallic cobalt catalyst generates bigger metallic particles, mainly located on the outer surface of the SBA-15 support and inactive for DRM reaction.

Interestingly, the bimetallic NiCo/SBA-15 catalyst does not present an intermediate catalytic performance but a dual behavior. Presenting an initial catalytic activity similar to that of monometallic nickel system, it quickly evolves to an inactive system, as is the case for the monometallic Co/SBA-15. This can be explained accepting

that the bimetallic cobalt nickel silicate formed after calcination mostly behaves as the monometallic nickel silicate, in the sense that it is mainly placed in the inner porous surface of the SBA-15 support, which yields after reduction small bimetallic particles into the mesoporous channels. However, it sinters during reaction showing that, unlike the nickel monometallic system, these bimetallic particles present a weak interaction with the SBA-15 support, and consequently, this interaction is mainly determined by cobalt. As a general conclusion, these findings suggest that cobalt should be segregated to the surface of these bimetallic entities, which interact weakly with the support, increasing their particle size under the harsh conditions of DRM reaction.

Acknowledgments

We thank the FEDER program and the "Ministerio de Economia y Competitividad" of Spain (Projects ENE2011-24412 and CTQ2014-60524-R) for funding this research. Also, we thank the ESRF facility and staff (BM25 SPLINE beamline) and ALBA facility and staff (BL22 CLAESS beamline) for their experimental support. A.R.G thanks also the Spanish Government for the PhD fellowship (BES-2012-061744).

References

1.- Pakhare, D.; Spivey, J., *Chemical Society Reviews*, 2014, 43, 7813-7837.

2.- Gonzalez-Delacruz, V. M.; Pereñiguez, R.; Ternero, F.; Holgado, J. P.; Caballero, A., *ACS Catalysis*, 2011, 1, 82–88.

3.- Espinos, J. P.; Gonzalez-Elipe, A. R.; Caballero, A.; Garcia, J.; Munuera, G., Journal of Catalysis, 1992, 136, 415-422.

4.- Batiot-Dupeyrat, C. ; Sierra Gallego, G.; Mondragon, F. ; Barrault, J. ; Tatibouet, J.M., Catalysis Today, 2005, 107–108, 474–480.

5.- Rostrup-Nielsen, J. R.; Nielsen, R., *Catalysis Reviews*, 2004, 46, 247-270.

6.- Rostrup-Nielsen, J.R.; Sehested, J.; Norskov, J.K., Advances in Catalysis, 2002, 47, 65-139.

7.- Matsumura, Y. ; Nakamori, T., Applied Catalysis A, General, 2004, 258, 107-114.

8.- Dong, W.; Roh, H.; Jun, K.; Park, S.; Oh, Y., Applied Catalysis A-General, 2002, 226, 63-72.

9.- Armor, J.N., Applied Catalysis A-General, 1999, 176, 159-176.

10.- Batiot-Dupeyrat, C. ; Valderrama, G. ; Meneses, A.; Martinez, F.; Barrault, J.; Tatibouet, J.M., Applied Catalysis A-General,2003, 248, 143-151.

11.- Y.H. Hu, E. Ruckenstein, Advances in Catalysis, 2004, 48, 297–345.

12.- Moctar, M.O.; Gonzalez-DelaCruz, V.M.; Colón, G.; Sebti, S.; Caballero, A., Applied Catalysis B: Environmental, 2014, 150, 459-465.

13.- Du, X.; Zhang, D.; Shi, L. Gao, R. ; Zhang, J., Nanoscale, 2013, 5, 2659-2663.

14.- Smolakova, L.; Kout, M.; Capek, L.; Rodriguez-Gomez, A.; Gonzalez-Delacruz, V.M.; Hromadko, L.; Caballero, A., International Journal of Hydrogen Energy, 2016, 41, 8459-8469.

15.- Chen, D.; Christensen, K.O.; Ochoa-Fernandez, E.; Yu, Z.X.; Totdal, B.; Latorre, N.; Monzon, A.; Holmen, A., Journal of Catalysis, 2005, 229, 82-96.

16.- Tang, S.; Ji, L.; Lin, J.; Zeng, H.C.; Tan, K.L.; Li, K., Journal of Catalysis, 2000, 194, 424-430.

17.- Liu, D.P.; Quek, X.-Y.; Wah, H.H.A.; Zeng, G.M.; Li, Y.D.; Yang, Y.H., Catalysis Today, 2009, 148, 243-250.

18.- Gonzalez-Delacruz, V. M.; Pereñiguez, R.; Ternero, F.; Holgado, J. P.; Caballero, A., Journal of Physical Chemistry C, 2012, 116, 2919-2926.

19.- Zhang, J.; Wang, H.; Dalai, A.K., Journal of Catalysis, 2007, 249, 300-310.

20.- Takanabe, K.; Nagaoka, K.; Nariai, K.; Aika,K.I., Journal of Catalysis, 2005, 232, 268-276.

21.- Wang, L.; Li, D.; Koike, M.; Watanabe, H.; Xu, Y.; Nakagawa, Y.; Tomishige, K., Fuel, 2013, 112, 654-661.

22.- Yu, C; Weng, W.; Shu, Q.; Meng, X.; Zhang, B.; Chen, X.; Zhou, X., Journal Natural Gas Chemistry, 2011, 20, 135-139.

23.- Silva, C.R.B.; Conceicao, L.; Ribeiro, N.F.P.; Souza, M.M.V.M., Catalysis Communications, 2011, 12, 665-668.

24.- Gonzalez-Delacruz, V. M.; Holgado, J. P.; Pereñiguez, R.; Caballero, A., Journal of Catalysis, 2008, 257, 307–314.

25.- Dias, J.A.C.; Assaf, J.M., Catalysis Today, 2003, 85, 59-68.

26.- Wang, N.; Xu, Z.X.; Deng, J.; Shen, K.; Yu, X.P.; Qian, W.Z.; Chu, W.; Wei, F., ChemCatChem, 2014, 6, 1470-1480.

27.- Vizcaíno, A. J.; Carrero, A.; Calles, J.A., Fuel Processing Technology, 2016, 146, 99-109.

28.- Oemar, U.; Kathiraser, Y.; Mo, L.; Hoa, X.K.; Kawi, S., Catalysis Science and Technology, 2016, 6, 1173-1186.

29.- Thielemann, J.P.; Girgsdies, F.; Schlögl, R.; Hess, C. Beilstein, Journal of Nanotechnology, 2011, 2, 110–118.

30.- Acatrinei, A. I., Hartl, M. A., Eckert, J., Falcao, E. H. L., Chertkov, G., Daemen, L. L., Journal of Physical Chemistry C, 2009, 113, 15634-15638.

31.- Zhao, D. Y., J. L. Feng, Huo, Q., Melosh, N., Fredrickson, G. H., Chmelka, B. F., Stucky, G. D., Science 1998, 279, 548-552.

32.- Liu, H., Wang, H., Shen, J., Sun, Y., Liu, Z., Applied Catalysis A-General, 2008, 337, 138-147.

33.- Malet, P.; Caballero, A., Chem Soc Faraday Trans 1988, 84, 2369-2375.

34.- Newville, M., Journal of Synchrotron Radiation, 2001, 8, 322.

35.- Li, J.F., Xia, C., Au, C.T., Liu, B.S., International Journal of Hydrogen Energy, 2014, 39, 10927-10940.

36.- Kong, X.; Zhu, Y.; Zheng, H.; Li, X.; Zhu, Y.; Li, Y.-W., ACS Catalysis, 2015, 5, 5914-5920.

37.- Albarazi, A., Gálvez, M. E., Da Costa, P., Catalysis Communications, 2015, 59, 108–112.

38.- Gálvez, M. E., Albarazi, A., Da Costa, P., Applied Catalysis A-General, 2015, 504, 143–150.

39.- Zhang, C.; Yue, H.; Huang, Z.; Li, S.; Wu, G.; Ma, X.; Gong, J., ACS Sustainable Chem. Eng., 2012, 1, 161−173.

40.- Rodriguez-Gomez, A.; Caballero, A., ChemNanoMat, 2017, 3, 94-97.

41.- Burattin, P., Che, M., Louis, C., Journal of Physical Chemistry B, 1997, 101, 7060-7074.

42.- Arcon, I.; Novak Tusar, N.; Ristic, A.; Kodre, A.; Kaucic, A., Physica Scripta, 2005, T115, 810–812.

43.- Grams, J.; Ura, A.; Kwapinski, W., Fuel, 2014, 122, 301-309.

Table 1

Specific surface areas and average pore size and average crystallite size of Ni/Co after calcination, reduction and DRM treatment.

	S_{BET} ($m^2 \cdot g^{-1}$) [Calc/red]	**Average pore size (nm)[a] [Calc/red]**	**Average crystallite size (XRD[b]) [Calc/*Red*]**	**Average particle size (TEM[c]) [*Red*/DRM]**
SBA-15	738	6.7	-	-
SBA-15-DP	249	9.1	-	
10% Ni/SBA-15	283/242	10.3/10.1	5.7/***4.1***	***4.3***/4.8
5-5% Ni-Co/SBA-15	261/232	12.0/11.1	7.0/***4.5***	***5.9***/7.7
10% Co/SBA-15	280/220	11.9/11.0	5.1/***13.2***	***14.4***/13.9

[a] Obtained by the BJH method.

[b] Calculed from the Scherrer equation for reduced samples.

[c] Obtained by sampling 150 particles.

Figure Captions

Figure 1. TEM images for calcined 10% Ni/SBA-15 (a), 5%-5% Ni-Co/SBA-15 (b) and 10% Co/SBA-15 (c).

Figure 2. XRD patterns of catalytic systems calcined (a) and treated in 5% H_2/Ar at 750 °C (b).

Figure 3. XANES spectra (left) and Fourier Transform functions of the EXAFS oscillations (right) of Ni K-edge (a) and Co K-edge (b) of calcined systems.

Figure 4. TPR profiles of the nickel and cobalt catalytic systems.

Figure 5. TEM images and particle size histograms of 10% Ni/SBA-15 (a), 5%-5% Ni-Co/SBA-15 (b) and 10% Co/SBA-15 (c), reduced in H_2 at 750 °C.

Figure 6. XPS spectra for calcined and *in situ* reduced 10% Co/SBA-15 (a) and 10% Ni/SBA-15 (b).

Figure 7. XPS spectra for calcined and *in situ* reduced 5%-5% Ni-Co/SBA-15.

Figure 8. CH_4 and CO_2 conversions in the reaction of DRM at 750 °C of the nickel and cobalt catalytic systems.

Figure 9. TEM images and particle size histograms of 10% Ni/SBA-15 (a), 5%-5% Ni-Co/SBA-15 (b) and 10% Co/SBA-15 (c), after DRM reaction at 750 °C.

Figure 1

Click here to download high resolution image

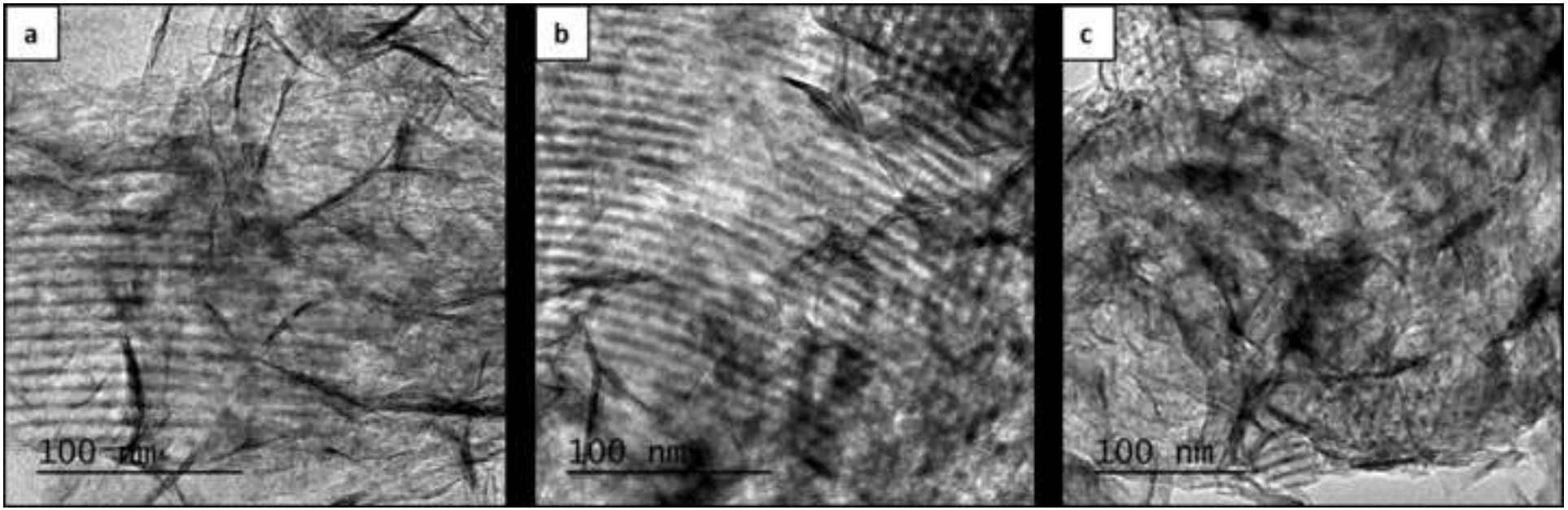

Figure 2

Click here to download high resolution image

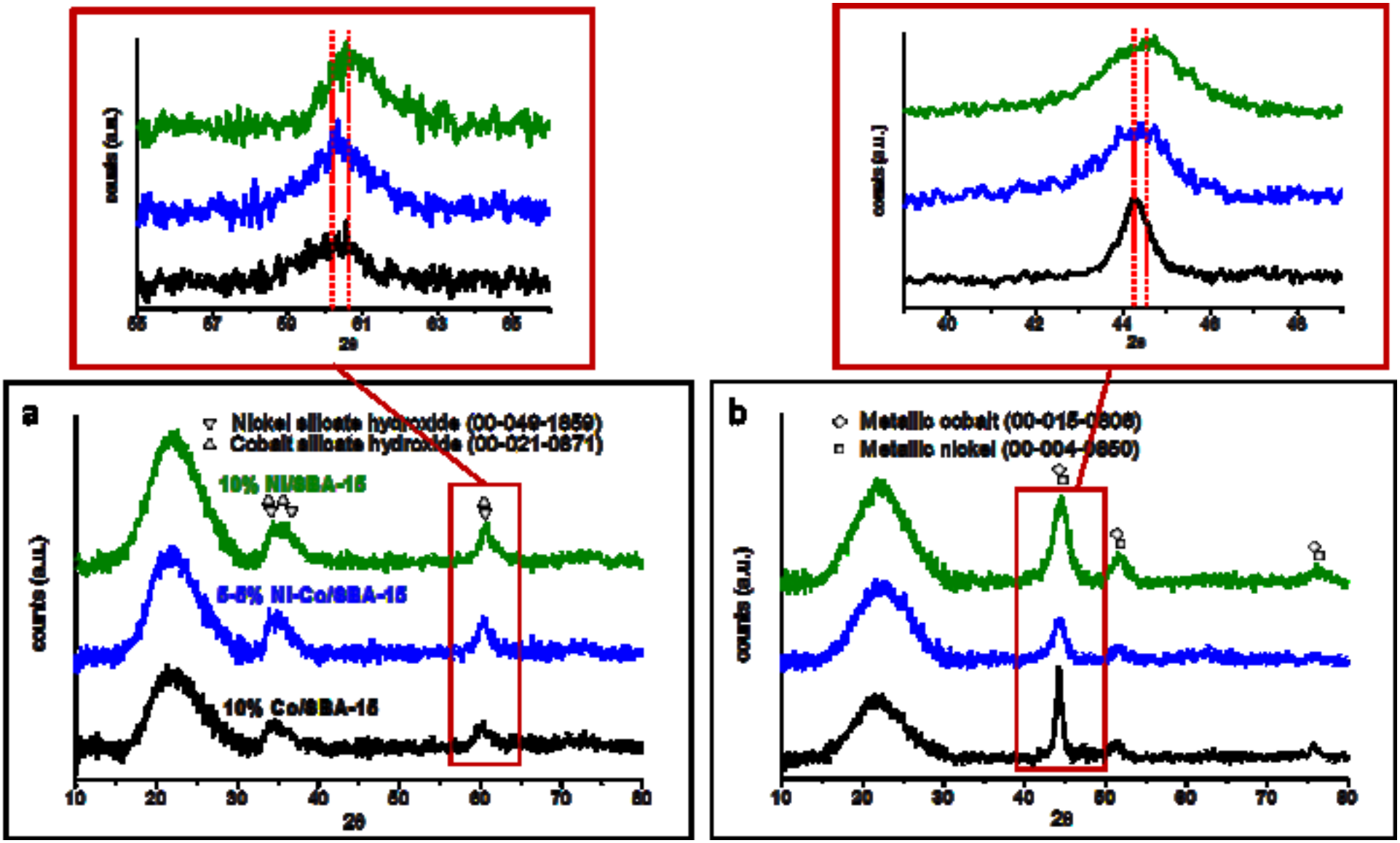

Figure 3

Click here to download high resolution image

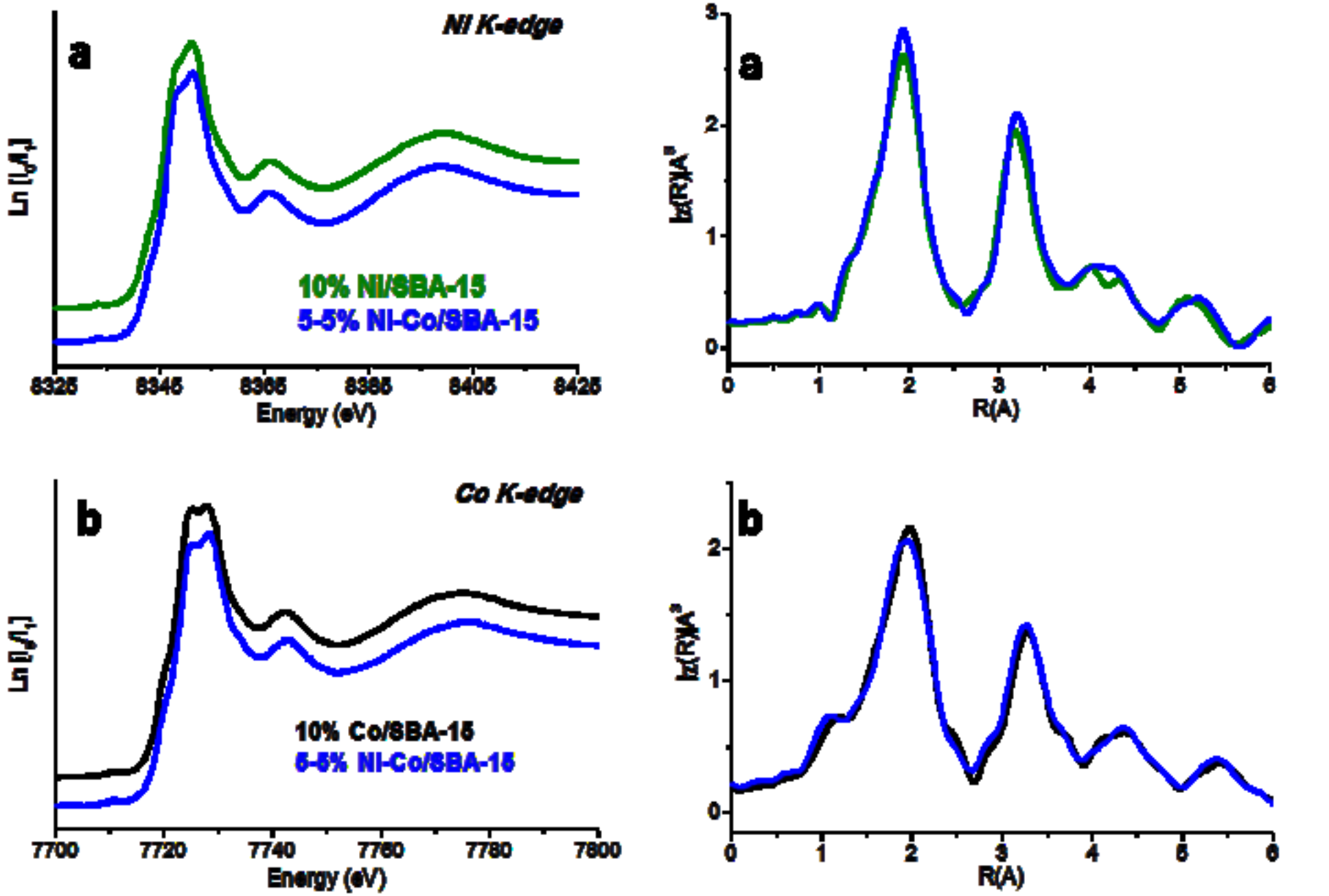

Figure 4

Click here to download high resolution image

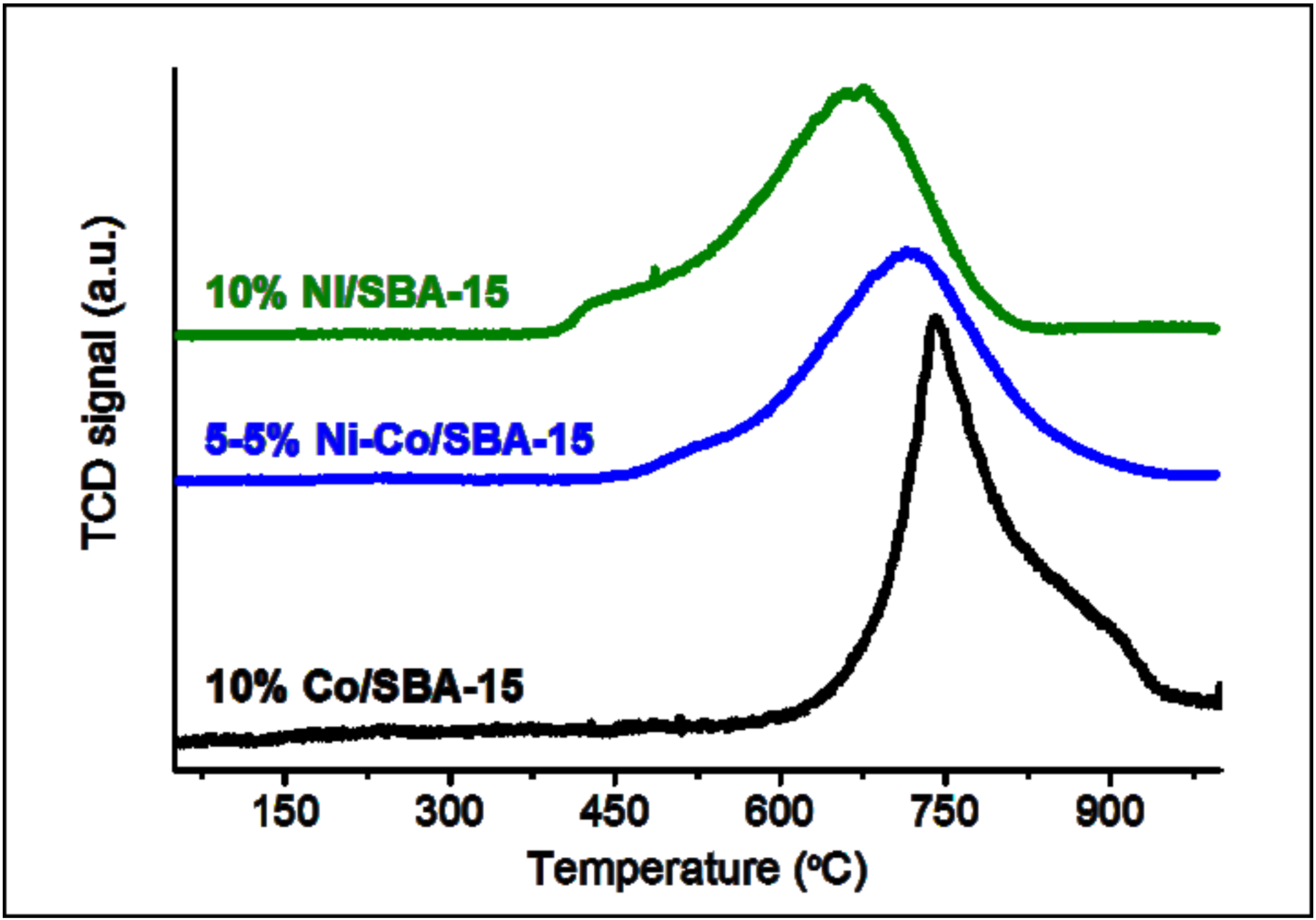

Figure 5

Click here to download high resolution image

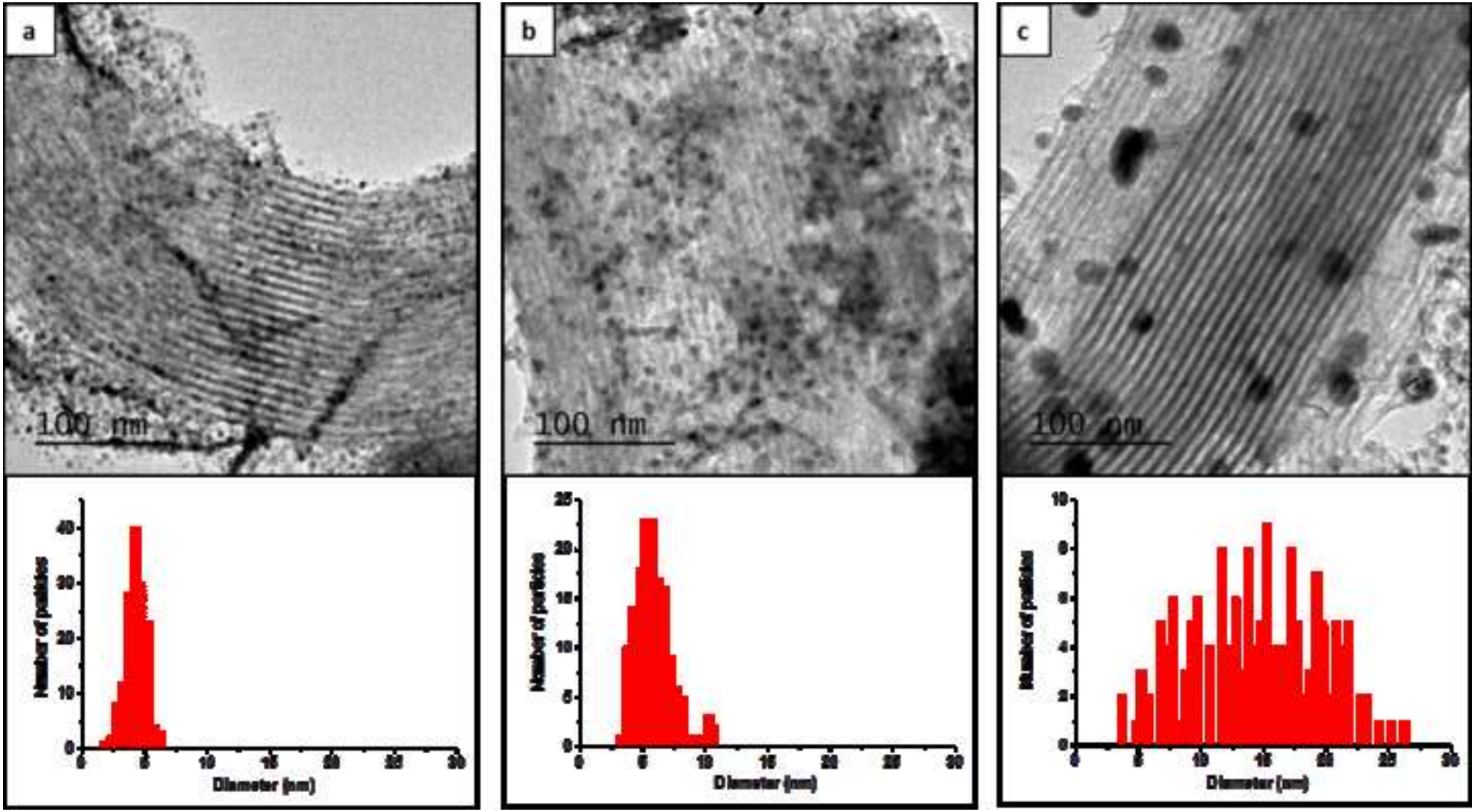

Figure 6

Click here to download high resolution image

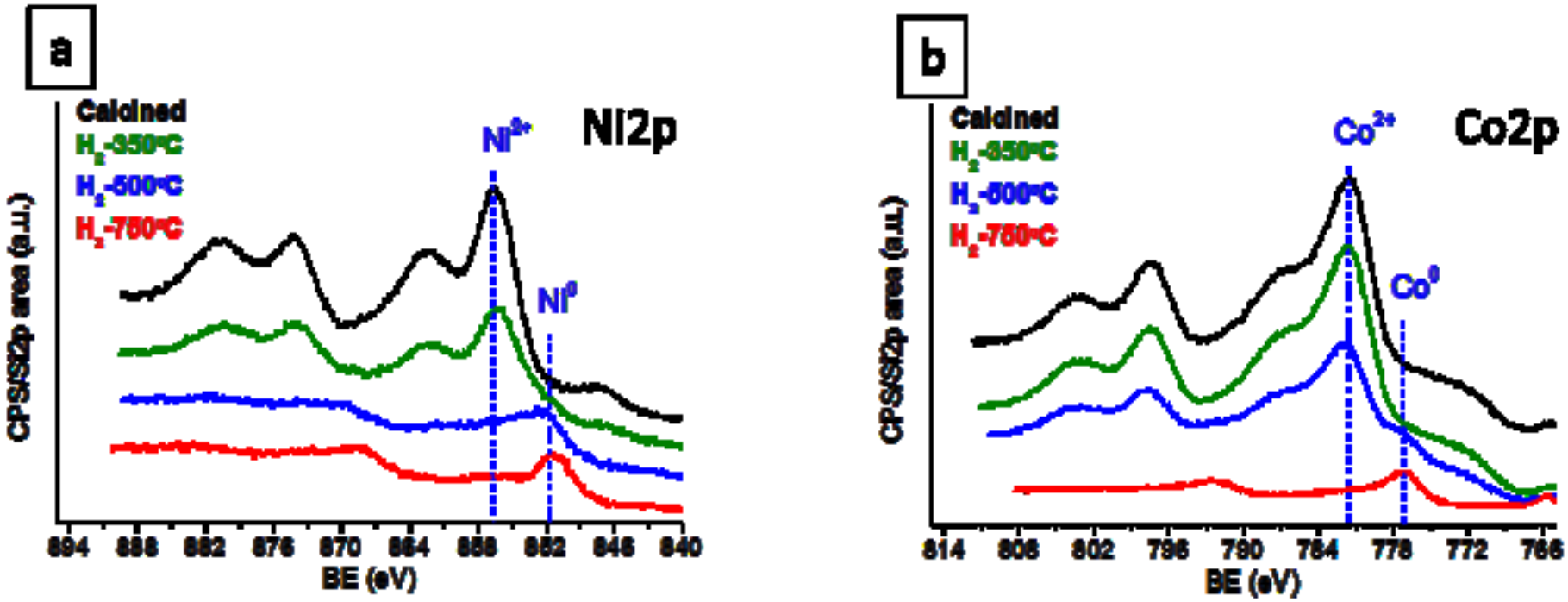

Figure 7

Click here to download high resolution image

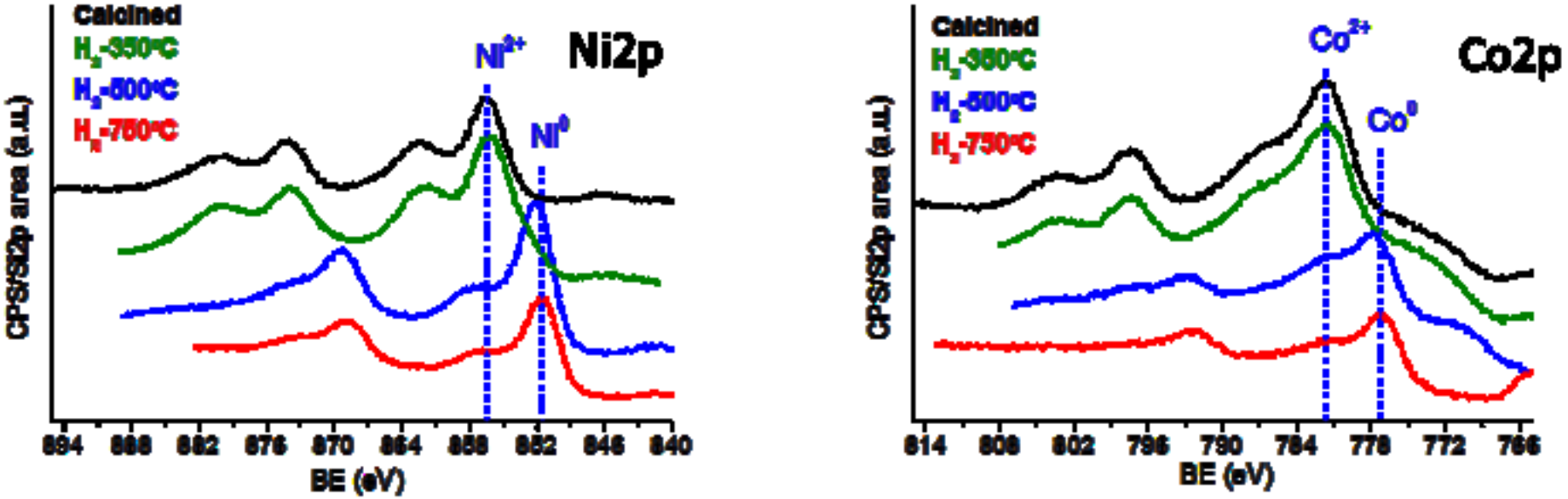

Figure 8

Click here to download high resolution image

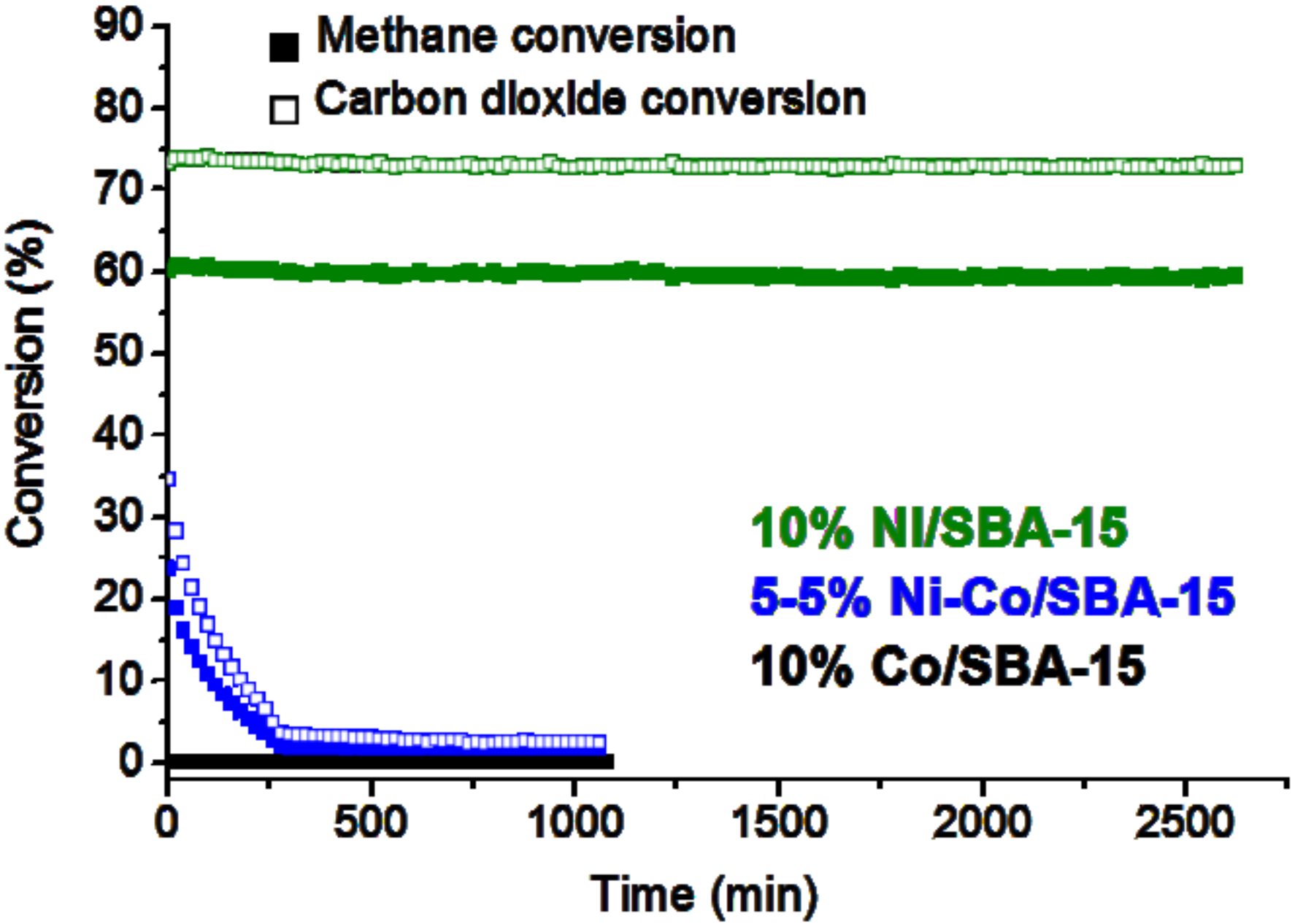

Figure 9

Click here to download high resolution image